# *A*-phase, field-induced tricritical point, and universal magnetocaloric scaling in EuPtSi

Ashish Kumar Mishra[*] and V. Ganesan

*UGC-DAE Consortium for Scientific Research, Indore 452001, MP, India*

Precise heat capacity $C(T, H)$ and electrical resistivity $\rho(T, H)$ down to 0.1 K and magnetic fields up to 10 T on EuPtSi is presented in detail. A detailed ($H$-$T$) phase diagram constructed, based on the $C(H)$ and $\rho(H)$ data, shows the presence of the *A* phase in EuPtSi, below a paramagnet-to-antiferromagnet/helimagnet transition $T_N \sim 4.1$ K. A clear entropy minimum across the *A* phase confirms the thermodynamic stability of the phase. Universal scaling performed using the change in magnetic entropy curves evidences the first-order transition below $T_N$ for magnetic fields lower than $H < 2.75$ T. The scaling analysis further suggests a field-induced second-order transition from paramagnet to a field-polarized state above $H > 3$ T, indicating a possible tricritical point at the boundary between a first-order and the field-induced second-order phase transition at $H_{TCP} \sim 2.75$ T and $T_{TCP} \sim 3.2$ K. The critical exponents $\beta \sim 0.5 \pm 0.05$, $\gamma \sim 0.97 \pm 0.04$, and $\delta \sim 3.23 \pm 0.14$ suggest that the EuPtSi belongs to a mean-field universality class, different from MnSi, which belongs to the universality class of the tricritical mean-field model.

## I. INTRODUCTION

Topological phases of matter have gained considerable interest in recent times. One such newly discovered "skyrmion" phase in the *H-T* phase diagram has been identified only for a handful of materials such as MnSi [1], FeGe [2], $Fe_{1-x}Co_xSi$ [3,4], $Cu_2OSeO_3$ [5,6], CoZnMn alloys [7], and for the systems in thin-film form [8,9]. In the prototype MnSi, earlier reports using neutron scattering suggested a helical structure below a paramagnet-to-helimagnet (PM-HM) transition $T_C \sim$ 29 K [10]. The skyrmion phase below $T_C$ has been probed through small-angle neutron scattering [1], the topological Hall effect [11], Lorentz transmission electron microscopy [4], ac susceptibility [12], and heat capacity [13,14]. Earlier theoretical arguments based on the different symmetry classes suggested the presence of Bloch and Néel-type skyrmions [15,16]. Though MnSi represents an early example of Bloch-type skyrmions [1,4], Néel-type skyrmions, however, have been reported only recently in some polar magnets such as $GaV_4S_8$ [17] and $GaV_4Se_8$ [18]. Moreover, antiskyrmions have also been observed in tetragonal Mn-Pt-Sn Heusler materials [19].

Another interest in the system is due to the presence of quantum phase transition (QPT) as a function of pressure [20] and doping [21]. Quantum phase transition is defined as the transition happening at $T$ tending to 0 K as a function of some nonthermal parameter such as pressure ($p$), doping ($x$), and magnetic field ($H$). With doping as a tuning parameter in $Mn_{1-x}Fe_xSi$ and $Mn_{1-x}Co_xSi$, $T_C$ is suppressed continuously to 0 K at a critical concentration of $x_C \sim 0.19$ and $x_C \sim 0.08$, respectively [21]. However, the continuous suppression of $T_C$ in MnSi [20] as a function pressure—at a critical pressure of $p_C \sim 14.6$ kbar—changes to first order

(FO) for the pressure range $p* < p < p_C$ ($p* \sim 12$ kbar) [22]. The deviation from the metallic Fermi liquid behavior [23] in the physical properties of $Mn_{0.75}Fe_{0.25}Si$ near a QPT has been attributed to the doping-induced spin fluctuations [24]. Similarly, enhancement of spin fluctuations has been noticed for the Cr-doped MnSi [25]. Also interesting is the observation of a tricritical point in MnSi from a first-order paramagnet to helimagnet to a field-induced second-order (SO) paramagnet to a field-polarized (PM-FP) state at $H_{TCP} \sim 340$ mT and $T_{TCP} \sim 28.5$ K [14]. A conclusion similar to that of Ref. [14] has been reached using a universal magnetocaloric (MCE) and magnetoresistance (MR) scaling [26]. The technique proves to be beneficial in determining the order of the transition.

A phenomenological approach employing the universal scaling of the change in magnetic entropy curves [27] for the compounds showing second-order phase transition has been developed and proved theoretically [28]. Nevertheless, the importance of such an approach is that in the absence of critical exponents the universal scaling curves could be constructed, which allows the change in magnetic entropy curves to collapse on to a universal master curve. Deviation from such behavior suggests the first-order nature of the transition and hence provides a unique way to identify the order of the phase transition. In a study [29] encompassing different systems with SO phase transition such as $TbCo_2$, $PrCo_2$, and $La_{2/3}Sr_{1/3}MnO_3$, the universal scaling is seen to hold over a wider temperature range of around $T_C$. The applicability of the model has been extended to the $RTiO_3$ ($R =$ rare earth) ferromagnetic compounds [30]. On the other hand, the critical scaling fails for systems showing first-order phase transition, such as $DyCo_2$, $HoCo_2$, and $La_{2/3}Ca_{1/3}MnO_3$ [29]. Importantly, a recent surge in materials showing large MCE needs to be tackled with options of rare-earth-based systems such as $Gd_5Si_2Ge_2$ [31], showing a giant MCE across the first-order transition. MnSi being a transition-based system shows a relatively small MCE [26]; hence the equivalent

rare-earth-based systems may provide a better option and need to be studied in light of their transport, thermodynamic, and magnetocaloric properties.

In addition, the search for materials with topological phases continues to draw attention due to their futuristic magnetic memory applications [32,33]. The natural candidate for the materials showing the skyrmion phase to look for would be the members with the same space group as that of MnSi. One such system, EuPtSi, recently attracted attention due to a possible presence of skyrmion phase in the phase diagram probed using magnetization and Hall resistivity [34]. However, earlier experimental results on EuPtSi [35] using Mössbauer and magnetization suggested the system to be paramagnetic down to 4.2 K. In contrast, a study using heat capacity and magnetization on polycrystalline EuPtSi suggests a fluctuation-induced first-order nature of the transition at $T_N \sim 4.1$ K [36]. Another study [37] using neutron diffraction on single crystals establishes the helical nature of the ground state and an additional phase transition of first-order nature accompanying hysteresis from commensurate to incommensurate at around 2.5 K. Moreover, a theoretical study on EuPtSi [38] considering the classical Heisenberg model suggests the ground state lies between a partially ordered state and frustrated state. Additionally, a Monte Carlo simulation performed predicts a first-order nature of the transition [39], and yet another theoretical study on EuPtSi [40] suggests a spin-ice state considering the ferromagnetic Ising model with local anisotropy.

The present study on polycrystalline EuPtSi shows a detailed $H$-$T$ phase diagram constructed using heat capacity $C(T, H)$ and electrical resistivity $\rho(T, H)$ measurements as a function of magnetic field and temperature down to 0.1 K. An interesting observation is the presence of a helimagnetic phase below $T_N$ in the $H$-$T$ phase diagram and a tricritical point separating a first-order paramagnet-to-helimagnetic transition ($H < 2.75$ T) from the field-induced second-order paramagnet to a field-polarized transition ($H > 3$ T). Additionally, universal MCE scaling performed above $H > 4$ T suggests the system belongs to a mean-field universality class.

The rest of the paper is organized as follows: The observation of the $A$ phase using electrical resistivity $\rho(H)$ and heat capacity $C(H)$ as a function of the magnetic field is presented in Sec. III A. Electrical resistivity $\rho(T)$ and heat capacity $C(T)$ as a function of temperature down to 0.5 and 0.1 K are presented in Secs. III B and III C, respectively. The MCE, MR, universal scaling, and critical exponents calculated are described in Sec. III D. A complete $H$-$T$ phase diagram incorporating the essential outcomes of the present finding is presented in Sec. III E.

## II. EXPERIMENTAL

A stoichiometric amount of elements from Alfa Aesar Eu (99.9%), Pt (99.9%), and Si (99.9%) were arc melted under the argon atmosphere, and sample homogeneity was ensured by melting it 3–4 times. The sample preparation conditions were similar to those described in Ref. [36]. Phase purity was confirmed on the powder sample using the Bruker D8 Advanced x-ray diffractometer (XRD). Heat capacity and dc electrical resistivity down to 2 K were measured using a QD

PPMS 2 K/14 T. The data below 2 K were recorded using the dilution refrigerator QD PPMS 0.05 K/16 T. Typically the error in heat capacity measurements at the lowest temperature for a zero field is always less than 0.15%, which under a magnetic field of 10 T is never more than 0.25%. However, the error in resistivity measurements at low temperatures for zero as well as magnetic field is less than 0.7%. The error bars in the heat capacity as well as electrical resistivity measurements are smaller than the symbols and was not considered further. A small piece of the sample of around 6 mg was used for the heat capacity measurement employing the relaxation method. The electrical resistivity measurements were performed on a bar-shaped sample using a linear four-probe method. The same sample after thinning was used for the ac resistivity measurement in a dilution refrigerator.

## III. RESULTS AND DISCUSSION

The crystal structure of EuPtSi belongs to a trillium lattice, which is highly frustrated owing to its geometry, where all the Eu atoms occupy $4a$ site forming a three-dimensional network of corner-sharing equilateral triangles [34,36,41]. The room temperature XRD performed on a polycrystalline sample is shown in Fig. 1 and is in line with the cubic $P2_13$ space group. The refinement performed using FULLPROF software provides the lattice parameter $a = 6.323(5)$ [36,41]. However, no traces of a secondary phase are observed within the experimental limits.

### A. *A* phase

Figure 2(a) shows the electrical resistivity $\rho(H)$ at various constant temperatures. The four distinct field-induced features $H_{C1}$, $H_{A1}$, $H_{A2}$, and $H_{C2}$ could be identified at 2 K [inset of Fig. 2(a)]. An initial slope change at around $H \sim 0.25$ T from antiferromagnetic/helimagnetic (AFM/HM) to a conical state is marked as $H_{C1}$. Additionally, a clear peaklike feature
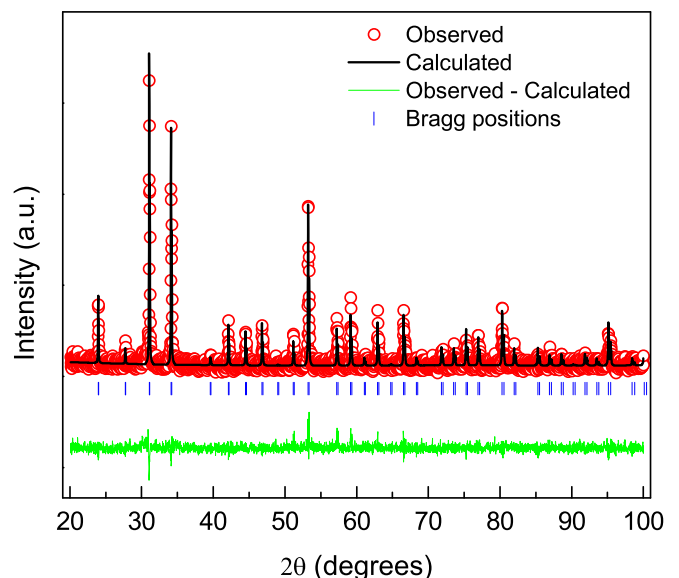


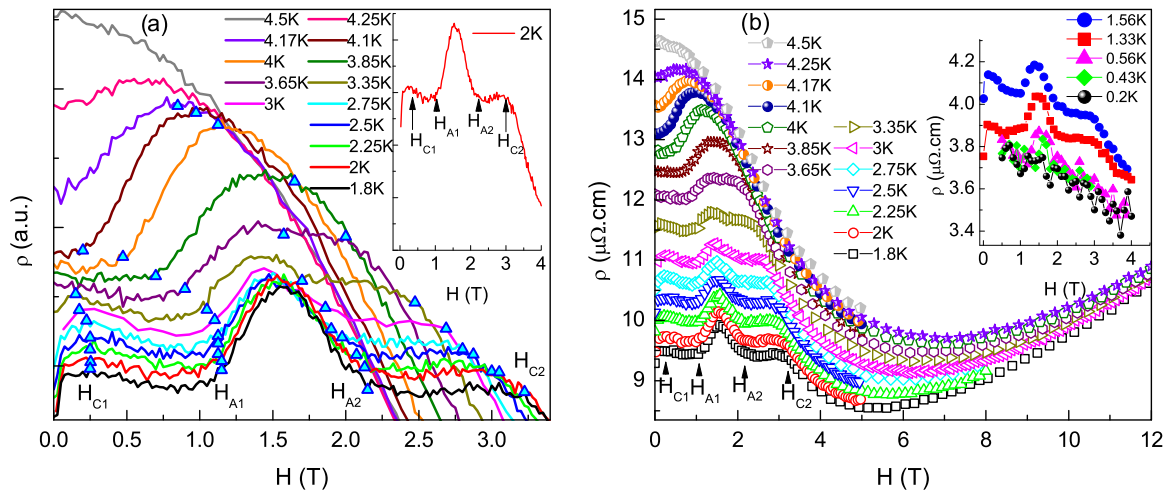FIG. 1. Room temperature XRD pattern for the polycrystalline sample of EuPtSi.

FIG. 2. Electrical resistivity $\rho(H)$ as a function of $H$ at given temperatures. (a) Region of $\rho(H)$ elaborating the different field-induced phases. The curves have been shifted by arbitrary units (a.u.). Inset: The 2-K data marked with arrows showing $H_{C1}$, $H_{A1}$, $H_{A2}$, and $H_{C2}$. (b) Same $\rho(H)$ data up to 12 T. Inset: Data collected using the dilution refrigerator from 1.56 down to 0.2 K.

observed between $H_{A1} \sim 1$ T and $H_{A2} \sim 2$ T denotes the contribution from the scattering of the conduction electrons of the $A$ phase and is line with the presence of an additional Hall effect in a similar field and temperature range [34]. A similar peaklike feature in resistivity is also reported for MnSi [42] and Fe$_{1-x}$Co$_x$Si [43]. However, a sudden drop in $\rho(H)$ at around $H_{C2} \sim 3$ T marks the transition from conical to a field-polarized state. The features corresponding to $H_{C1}$, $H_{A1}$, and $H_{A2}$ move to the lower values with an increase in temperature and diminish completely above 3.65 K, whereas $H_{C2}$ persists up to 4.17 K. The inset of Fig. 2(b) shows the data below 1.8 K and down to 0.2 K. The signatures of the $A$ phase are visible down to 0.43 K; however, no such feature could be seen at $T = 0.2$ K. Furthermore, all the curves in Fig. 2(b) show almost a similar trend, except for the field region below $H_{C2}$. The $\rho(H)$ in the PM phase above $T \sim 4$ K shows a decreasing trend, which suggests the suppression of spin fluctuations with an increase in the magnetic field. However, above 7 T, the $\rho(H)$ starts to increase with a field that is compatible with the orbital motion of the conduction electrons.

Figures 3(a) and 3(b) show $C/T$ plotted as a function of $H$ for different temperatures near and below $T_N$. The features corresponding to $H_{C1}$, $H_{A1}$, $H_{A2}$, and $H_{C2}$ could be observed in the $C/T$ with increasing $H$ and are shown for 2 K in Fig. 3(a). As could be seen in Fig. 3(b), a clear maximum at around $H_{C2} \sim 0.8$ T, at 4 K, in contrast to the featureless curve at 4.5 K, shows the field-induced transition from conical to a field-polarized state. In addition, a broad humplike feature starts to appear at 3.75 K at around 1.2 T that further splits into two peaks corresponding to $H_{A1}$ and $H_{A2}$ at 3.25 K and persists down to 0.6 K. However, no features related to $H_{A1}$ or $H_{A2}$ could be seen at $T = 0.35$ K. A local minimum observed between $H_{A1}$ and $H_{A2}$ suggests the low entropy state of the $A$ phase inside the conical phase. Moreover, keeping in mind the entropy variation corresponding to the $A$ phase, heat capacity provides an important tool to establish the thermodynamic nature of the phase [13,14]. Nonetheless, the features observed corresponding to $H_{C1}$, $H_{A1}$, $H_{A2}$, and $H_{C2}$ are in line with the $\rho(H)$ measurement.
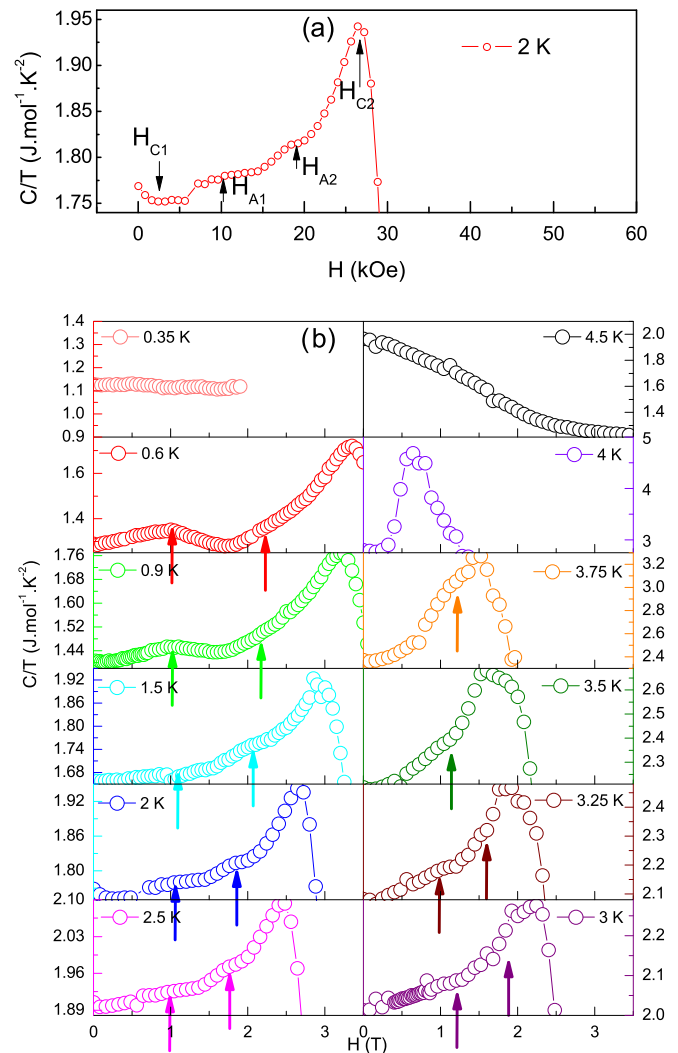


FIG. 3. (a) $C/T$ as a function of $H$ at 2 K with arrows marking $H_{C1}$, $H_{A1}$, $H_{A2}$, and $H_{C2}$. (b) A part of $C/T$ vs $H$ depicting the features related to the $A$ phase. The arrows mark $H_{A1}$ and $H_{A2}$.
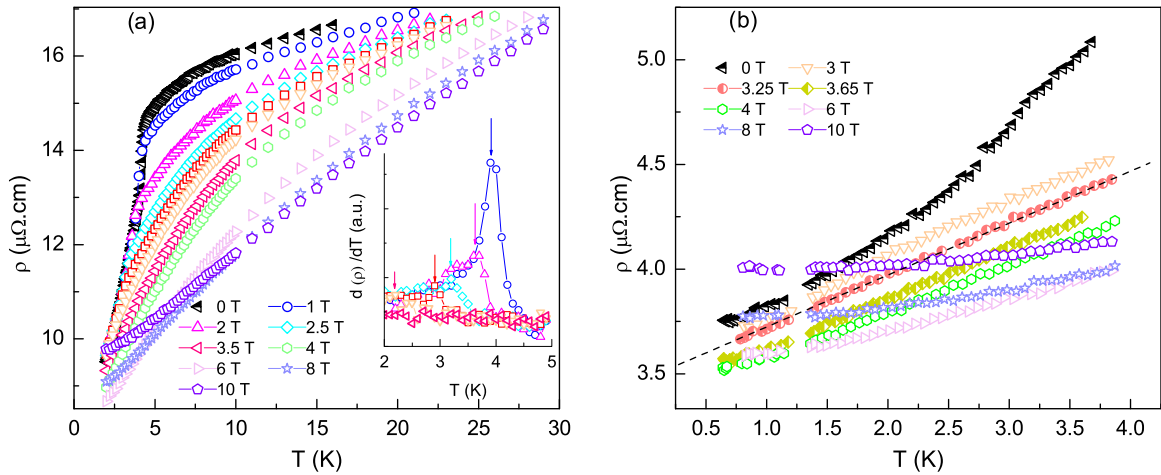
FIG. 4. (a) dc electrical resistivity $\rho(T)$ as a function of $T$ down to 2 K for different fields up to 10 T. Inset: The derivative with respect to $T$ at given fields. The arrows mark the variation of $T_N$. (b) ac resistivity in the range 4–0.5 K using a dilution refrigerator under different constant fields. The dashed line represents a linear behavior.

## B. Resistivity

The metallic nature of the system is evidenced using the resistivity measurement. The PM-AFM/HM transition manifests as a sharp drop of resistivity at around 4.1 K and is line with the other reports [34,41]. The drop in resistivity below $T_N$ suggests the ordering of the spins and a reduction in spin fluctuation scattering of the conduction electrons.

Figures 4(a) and 4(b) show the ac and dc electrical resistivity $\rho(T)$ as a function of $T$ down to 2 and 0.5 K, respectively. The derivative of $\rho(T)$ plotted against $T$ [inset of Fig. 4(a)] shows the transition at $T_N$ moves to lower temperatures with an increase in field values, and no transition could be observed for $H > 3$ T down to 2 K. However, to ensure the variation of $T_N$ below 2 K, the measurements were extended down to 0.5 K using the dilution refrigerator. The transition for $H = 3$ T is evident as a slope change at around 2 K; on the other hand, no features related to the transition could be observed down to 0.5 K for the $H > 3$ T field. Nevertheless, a linear-in-$T$ behavior could be seen for $H = 3.25$ T [Fig. 4(b)], typical of scattering due to a degenerate ground state of $Eu^{2+}$ [34].

Figures 5(a) and 5(b) show the resistivity as a function of $T^2$ for different constant fields. The linear-in-$T^2$ behavior down to the lowest temperature starts to evolve for the fields above $H \geqslant 4$ T and moves to a higher temperature with an increase in magnetic field. The $T^2$ behavior typical of a metallic ground state suggests the recovery to a Fermi liquid behavior [23] in the FP state.

## C. Heat capacity

Heat capacity $C(T)$ as a function of $T$ for different fields down to 0.1 K is shown in Fig. 6. A sharp peak at 4.1 K shows the PM-AFM/HM transition and is in agreement with the earlier reports [36,41]. The sharp peak at $T_N$ first moves towards the lower temperature with an increase in field values and changes its shape at and above around 2.75 T. However, the peak get completely smeared at 3.5 T, above which a broad humplike feature appears and starts to move towards a higher temperature with an increase in the field values, suggesting a field-induced PM-FP transition. The low-temperature part of
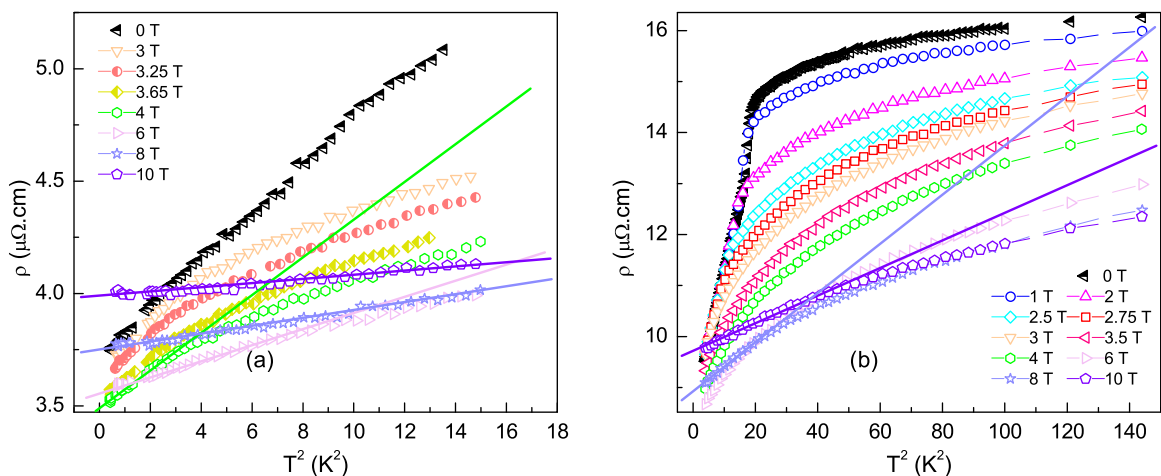


FIG. 5. $\rho(T)$ as a function of $T^2$ for different fields up to 10 T. (a) ac resistivity in the range 4–0.5 K. (b) dc resistivity down to 2 K. The solid line represents the linear fit in $T^2$.
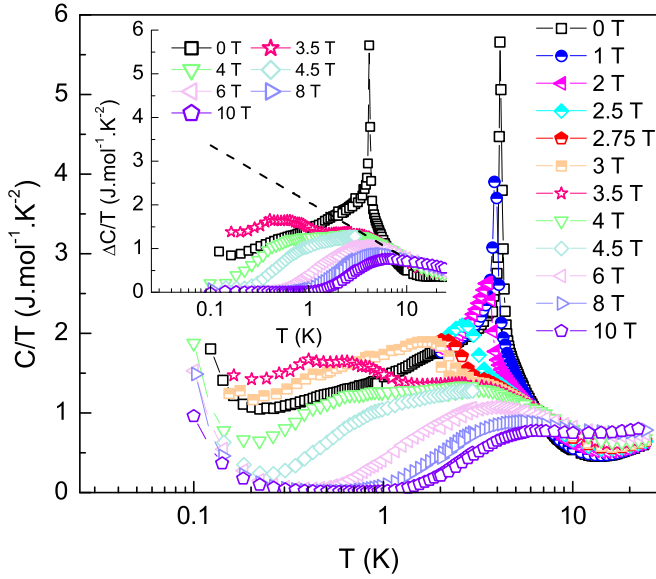
FIG. 6. $C(T)$ as a function of $T$ down to 0.1 K on the semilog scale for different fields up to 10 T. Inset: Data with nuclear and lattice part subtracted on the semilog scale. The dashed line represents a $-\ln T$ behavior.
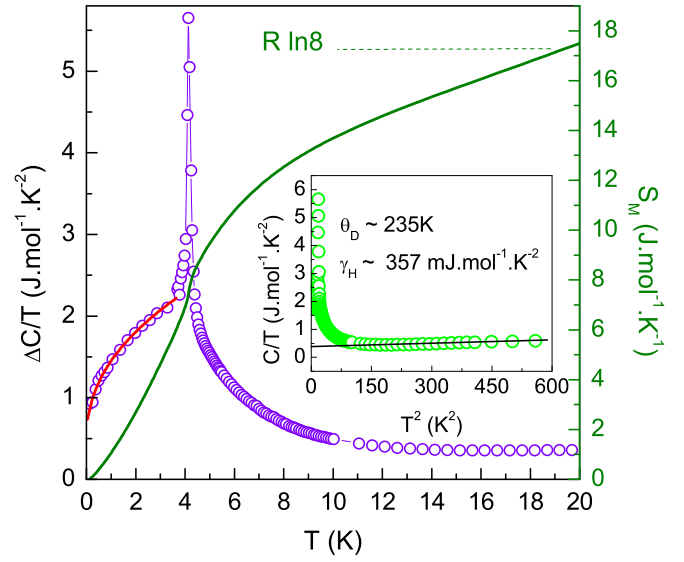


FIG. 7. Left scale: $\Delta C/T$ plotted vs $T$ down to 0.1 K. The solid red line at low temperatures is a fit to a spin wave below $T_N$ as described in the text. Right scale: Absolute entropy $S_M$ as a function of $T$, calculated using Eq. (1a). Inset: $C/T$ as a function of $T^2$. The solid black line represents a linear fit in $T^2$.

the heat capacity shows an upturn which could be attributed to a nuclear Schottky effect. The effect has been subtracted from the data in the form of $C_{Sch} \sim \alpha/T^2$ [44] (inset of Fig. 6), where the term approximates the high-temperature tail of the Schottky hump. Additionally, the AFM systems with low $T_N$ are known to show a field-induced QPT-like behavior in YbRh$_2$Si$_2$ [45] and CeCu$_{6-x}$Ag$_x$ [46], and signatures of the same have been looked for in the present system. However, the possibility of a field-induced QPT could be neglected, as the $\Delta C/T$ vs $T$ (inset of Fig. 6) does not show any logarithmic behavior [47] down to the lowest temperature for any given field. Nevertheless, the symmetric peak in $C(T)$ and the sharp features corresponding to the transition in $\rho(T)$ and $C(T)$ comparable to that of the single crystal [34,36,41] show the good quality of the present sample and may suggest a FO nature of the transition.

$\Delta C/T$ plotted as a function of $T$ for zero fields down to 0.1 K is shown in Fig. 7 (left scale). The lattice contribution has been subtracted in the form $C/T = \gamma_H + \beta T^2$, where $\gamma_H$ denotes the Sommerfeld coefficient at high temperatures and $\beta$ denotes the lattice contribution. However, due to the presence of a magnetic peak at low temperature, the fit was performed above 12 K (inset of Fig. 7). The obtained Debye temperature from the fit, using the relation $\theta_D = (5\beta/12R\pi^4)^{-1/3}$, is $\theta_D \sim 235$ K, and the Sommerfeld coefficient at high temperature is $\gamma_H \sim 357$ mJ mol$^{-1}$ K$^{-2}$. However, the low-temperature data below $T \sim 3.5$ K was fitted with a ferromagnetic spin-wave contribution using the relation $\Delta C/T = \gamma_L + \delta_{SW} T^{1/2} \exp(-\Delta/T)$, which resulted in a somewhat higher value of $\gamma_L \sim 725$ mJ mol$^{-1}$ K$^{-2}$, and may suggest the system to be a heavy fermion, as is true for other Eu-based systems [48,49]. Here $\gamma_L$ denotes the Sommerfeld coefficient at low temperatures, $\delta_{SW}$ is the coefficient of $T^{3/2}$ term that represents the ferromagnetic component of heat capacity, and $\Delta$ represents the gap in the spin-wave excitation

spectrum. The large value of $\delta_{SW} \sim 805$ mJ mol$^{-1}$ K$^{-5/2}$ and small value of the spin-wave gap $\Delta \sim 0.1$ K suggests the softer magnons and a small anisotropy gap present in the system. The absolute entropy $S_M$ calculated using Eq. (1a) is shown in Fig. 7 on the right scale. The total entropy at $T_N$ amounts to only half the value of $R\ln 8$ expected for $J = 7/2$ of Eu$^{2+}$. However, the full entropy is recovered at around 20 K, which may suggest the presence of short-range order or fluctuations above $T_N$ [34,36]:

$$S_M = \int_0^T \frac{C}{T'} dT', \tag{1a}$$

$$\Delta S_M = S_M(H, T) - S_M(0, T). \tag{1b}$$

### D. MCE, MR, and universal scaling

Figure 8(a) shows MCE ($-\Delta S_M$) as a function of $T$, where MCE is calculated using Eq. (1b), where $S_M(H, T)$ denotes the entropy calculated under the magnetic field, and $S_M(0, T)$ denotes the entropy calculated under zero field. The MCE observed in EuPtSi amounts to the maximum value of 6 J mol$^{-1}$ K$^{-1}$ at a field change of 10 T, which for MnSi is around 0.40 J mol$^{-1}$ K$^{-1}$ at 10 T [26]. The MCE below $T_N$ shows a negative trend; however, the trend changes to positive above $T_N$, with a maximum at around 5 K for the field change of 1 T. The maximum in $-\Delta S_M$ moves to higher $T$ with an increase in the field values. Moreover, the negative trend is not visible above 3 T. A similar MCE behavior is reported for the case of MnSi [50], and the similarity is quite remarkable for the two systems. Both systems show a negative $-\Delta S_M$ in low fields that changes to positive $-\Delta S_M$ above a certain field, which for MnSi is 1 T and for EuPtSi is 3 T.

Figure 8(b) shows MR as a function of $T$ and is calculated using the relation $\Delta\rho = \{[\rho(H) - \rho(0)]/\rho(0)\} \times 100$. A maximum MR of around 35% is observed at a field change
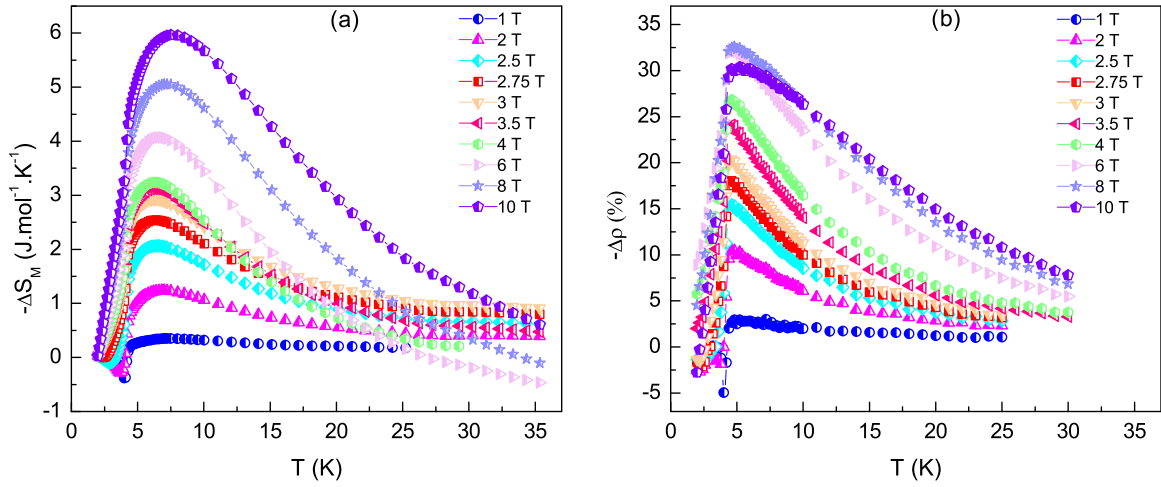
FIG. 8. (a) MCE and (b) MR as a function of $T$ for different constant fields up to 10 T.

of 10 T, which for MnSi is around 40% at 10 T [26]. The MR shows a similar behavior to MCE, showing a negative trend below $T_N$ and changing its behavior to positive above $T_N$, with a maximum at around 5 K for the field change of 1 T:

$$\theta = \left\{ -\frac{T - T^P}{T - T_{r_1}} \right\}, \quad T \leqslant T^P, \tag{2a}$$

$$\theta = \left\{ \frac{T - T^P}{T - T_{r_2}} \right\}, \quad T > T^P. \tag{2b}$$

Figure 9 shows the normalized magnetic entropy change $\Delta S' = -\Delta S_M/\Delta S_M^P$ ($\Delta S_M^P$ is the peak value) as a function of reduced temperature $\theta$, calculated using Eq. (2), where $T^P$ is the peak temperature, and $T_{r_1}$ and $T_{r_2}$ are the reference temperatures [27]. The data shows a good collapse of the different magnetic entropy change curves on to the universal
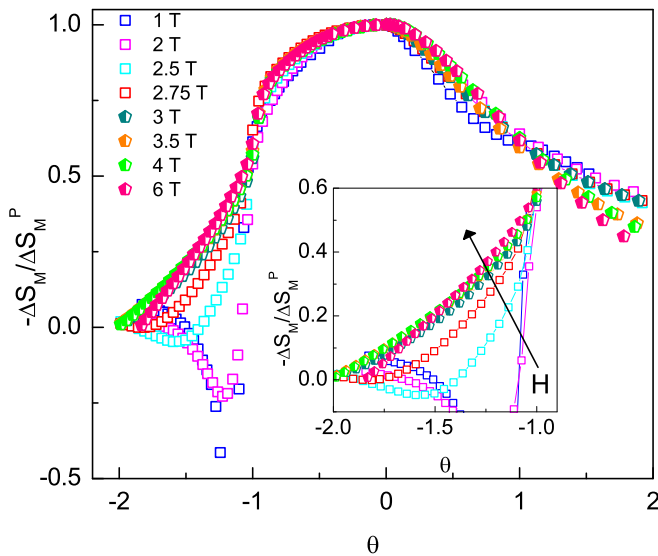
master curve. However, the data below $\theta < -1$ does not overlap and shows a considerable deviation. Such behavior has been found experimentally for the systems showing a FO phase transition [29]. Moreover, the deviation from the master curve is observed only for fields $H < 3$ T, while the data for fields $H > 3$ T converge on to the universal master curve, suggesting the field-induced SO phase transition.

Figures 10(a) and 10(b) show the field dependence of $\Delta S_M^P$ and RCP, where RCP is relative cooling power and was calculated using the relation RCP $= \Delta S_M^P \times \delta T_{FWHM}$ (here $\delta T_{FWHM}$ is the full width at half maxima). The points were fitted with Eqs. (3) and (4), providing the values of $n \sim 0.69$ and $\delta \sim 3.23$. Considering the critical exponents from the mean-field model, $\beta = 0.5$, $\gamma = 1$, and $\delta = 3$ give $n \sim 0.69$, close to the value obtained from the field dependence of $\Delta S_M^P$:

$$|\Delta S_M|^P \propto H^n, \tag{3}$$

$$\text{RCP} \propto H^{1+\frac{1}{\delta}}, \tag{4}$$

$$n = 1 + \frac{1}{\delta}\left(1 - \frac{1}{\beta}\right), \tag{5a}$$

$$n = 1 + \left[\frac{\beta - 1}{\beta + \gamma}\right]. \tag{5b}$$

The critical exponents calculated using Eqs. (5a) and (5b) are $\beta \sim 0.5 \pm 0.05$, $\gamma \sim 0.97 \pm 0.04$, and $\delta \sim 3.23 \pm 0.14$,
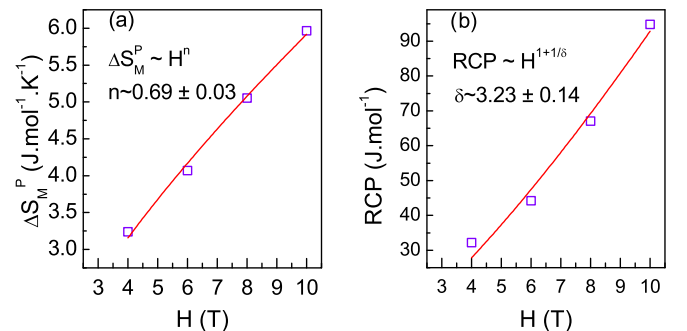


FIG. 9. Normalized magnetic entropy change $\Delta S' = -\Delta S_M/\Delta S_M^P$ as a function of reduced temperature $\theta$. Inset: Region where scaling is violated. The arrow shows the increase in field values.



FIG. 10. (a) $\Delta S_M^P$ and (b) RCP as a function of $H^n$. The corresponding solid lines are the fits using Eqs. (3) and (4).

TABLE I. Comparison between the critical exponents obtained for EuPtSi and MnSi through MCE and modified Arrott plot (MAP) scaling. Here, $\beta$, $\gamma$, $\delta$, and $n$ are the critical exponents. The values of $\delta$ and $n$ for EuPtSi are obtained through the fits using Eqs. (3) and (4). However, the values of $\beta$ and $\gamma$ are calculated using Eqs. (5a) and (5b). PC: polycrystal, SC: single crystal.

| Compound | Technique | $\beta$ | $\gamma$ | $\delta$ | $n$ | Reference |
|---|---|---|---|---|---|---|
| EuPtSi[PC] | MCE scaling | $0.5 \pm 0.05$ | $0.97 \pm 0.04$ | $3.23 \pm 0.14$ | 0.69 | This work |
| MnSi[PC] | MCE scaling | $0.25 \pm 0.02$ | $1.29 \pm 0.27$ | $6.18 \pm 0.28$ | 0.51 | [26] |
| MnSi[PC] | MAP | 0.238(1) | 1.20(1) | 6.10(1) | | [51] |
| MnSi[SC] | MAP | 0.242(6) | 0.915(3) | 4.734(6) | | [52] |

which are close to the exponents corresponding to the mean-field model. On the other hand, the exponents for the MnSi, obtained through different techniques [26,51,52], belong to the tricritical model and are tabulated in Table I. Additionally, the reliability of the exponents obtained can be further confirmed through the scaling equation of state based on the assumption of scaling near the SO phase transition, where the magnetic equation of state is given by [53–55]

$$\frac{H}{M^\delta} = h\left(\frac{\varepsilon}{M^{1/\beta}}\right), \qquad (6)$$

where $\varepsilon$ is the reduced temperature $\varepsilon = (T - T_C)/T_C$, $T_C$ is the Curie temperature, $M$ is the magnetization, $H$ is the applied field, and $h(x)$ is a scaling function. The scaling equation of state for the case of magnetic entropy change could be written as [28]

$$\frac{\Delta S_M}{a_M} = H^{\frac{1-\alpha}{\Delta}} s\left(\frac{\varepsilon}{H^{\frac{1}{\Delta}}}\right), \qquad (7)$$

where $\Delta = \beta\delta$, $a_M = T_C^{-1} A^{\delta+1} B$ [$A$ and $B$ are the critical amplitudes related to [$M = A(-t)^\beta$] and ($H = BM^\delta$)], and $s$ is the scaling function [28,29]. The universal scaling curves based on Eq. (7) are plotted in (a). The excellent collapse of different magnetic entropy change curves onto the universal curve confirms the reliability of the critical exponents obtained.

Figure 11(b) shows $\Delta S'$ as a function of $\theta$ for the fields $H > 4$ T. The data for different entropy curve changes shows a good collapse onto the universal master curve, suggesting the SO nature of the transition above $H > 4$ T and is in agreement with the other systems, Ref. [29] and references therein. Nevertheless, a small dispersion ($d$) at around $\theta < -1.5$ has been quantified using Eq. (8):

$$d = \frac{W(\theta = -1.5)}{\Delta S'(\theta = -1.5)} \times 100, \qquad (8)$$

where $W$ is the vertical displacement of the data point at $\theta = -1.5$ from the mean value of $\Delta S'(\theta = -1.5)$. The maximum dispersion is about 30% and is in accordance with Ref. [29], where the systems with SO phase transition show the dispersion to be less than 30%, while systems showing FO phase transition show a dispersion of greater than 100%. Moreover, a similarity in the temperature dependence of MCE and MR is exploited to perform a universal scaling with MR and is shown in Fig. 11(c). The scaling again collapses well onto the master curve. In addition to that, Fig. 11(d) compares the universal MCE scaling for MnSi [26] and EuPtSi. The two data sets are seen to diverge below $\theta < 0$ and suggests that the

systems belong to two different universality classes. This is further evidenced by the critical exponents obtained above for the case of EuPtSi, which belongs to the mean-field model that is different from that of MnSi, which belongs to the tricritical mean-field model. The critical exponents obtained through various methods are compared in Table I. It is pertinent to note that the validity of the universal scaling holds, provided the crystallite size is larger than the diverging correlation length at $T_C$ and the sample is homogeneous and uniform. However, the polycrystalline nature of the sample may hinder the critical scaling in the limit where the correlation length exceeds the crystallite size near the critical region [56,57]. Nevertheless, universal scaling for EuPtSi seems reasonable considering the uniform and homogeneous nature of the sample, as is evidenced through the sharp transitions as well as the value of $T_C$, which is in agreement with the single-crystal data [34,36,41]. Similar universal scaling on polycrystalline
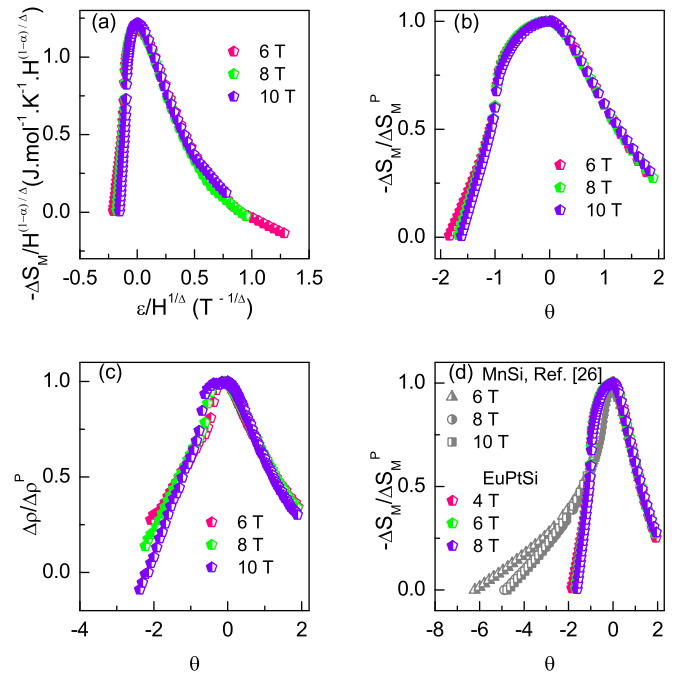


FIG. 11. (a) Universal scaling performed based on the equation of state using Eq. (7). (b) Normalized magnetic entropy change as a function of reduced temperature $\theta$. (c) Similar scaling with the MR data, where $\Delta\rho' = \Delta\rho/\Delta\rho^P$. (d) Comparing the universal MCE scaling for MnSi [26] and EuPtSi. Divergence in the low-temperature ($\theta$) range between two data sets shows the systems to belong to two different universality classes.
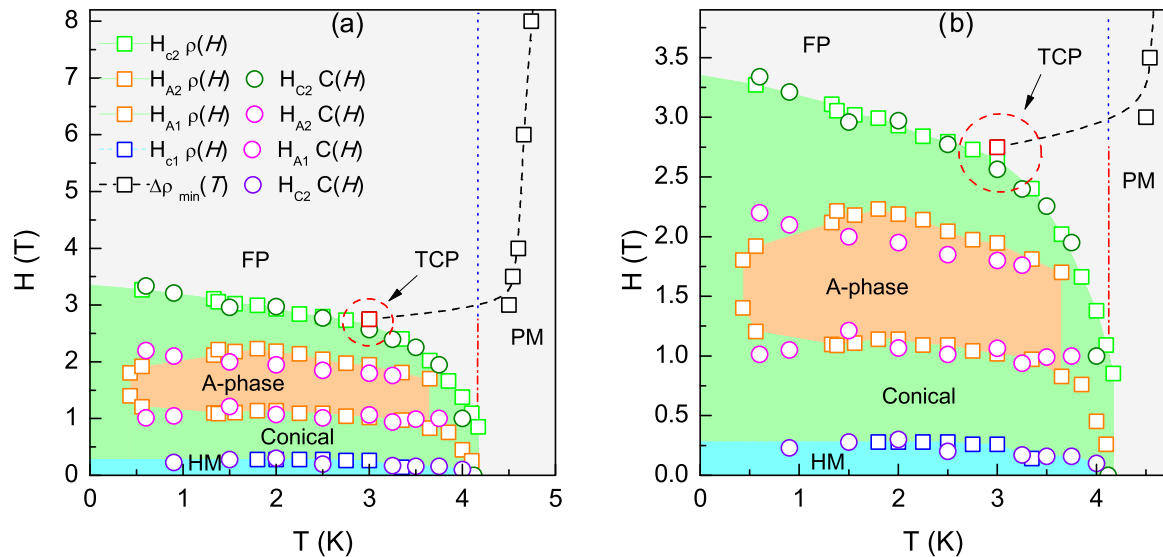
FIG. 12. (a) $H$-$T$ phase diagram constructed using $C(H)$ and $\rho(H)$. (b) A close-up view near the tricritical point (marked with a dashed red circle). The red dashed-dotted line below $H \sim 2.75$ T marks the $T$ range below which universal MCE scaling fails. The blue dotted line above $H \sim 2.75$ T marks the $T$ range below which universal MCE scaling holds.

MnSi [26,51] and other polycrystalline samples (Ref. [51] and references therein) [56] has already been reported in the literature. Moreover, due to lack of reports on universal scaling in single-crystal EuPtSi, the issue cannot be concluded unambiguously. To further confirm the value of the critical exponents, a study on a single crystal is surely required.

### E. *H-T* phase diagram

Figures 12(a) and 12(b) show the *H-T* phase diagram. The data points were taken from the $C(H)$ and $\rho(H)$ measurements as a function of magnetic fields at different temperatures. A cascade of field-induced transitions below $T_N$ could be observed with an increase in the magnetic field. For example, at $T = 1$ K, increasing the magnetic field results in a transition from helical to conical phase at $H_{C1} \sim 0.25$ T then from conical to $A$ phase at $H_{A1} \sim 1$ T and from $A$ phase back again to conical phase at $H_{A2} \sim 2$ T. Increasing the magnetic field above $H_{C2} \sim 3.2$ T results in a transition from conical to FP state. A clear $A$-phase pocket which is closed in $H$-$T$ space could be seen below $T_N$. The suitability of EuPtSi to host a possible skyrmion phase roots from the $P2_13$ space group, which lacks the inversion symmetry—a desired property for materials to have Dzyaloshinskii-Moriya (DM) interaction [58,59]—and may provide a rare example from the rare-earth-based $f$-electron systems. As far as the true ground state below $T_N$ is concerned, a clear signature corresponding to the field-induced transition from helical to conical phase at around $H_{C1} \sim 0.2$ T in $C(H)$ and $H_{C1} \sim 0.25$ T in $\rho(H)$ suggests the ground state in zero fields to be HM, similar to MnSi. Moreover, the similarity in $M$ vs $H$ to the MnSi, except for the saturation field shifted to higher values and the absence of a sudden and sharp metamagneticlike transition [34,36], discards the true AFM order below $T_N$. The absence of sudden metamagneticlike transition may result from the system being already in a spin-flopped state (canted phase). Obviously, the higher value of the saturation field

from conical to FP state in EuPtSi ($H_{C2} \sim 2.66$ T at 2 K) [34] in comparison to MnSi ($H_{C2} \sim 0.6$ T at 2 K) [21] indicates the larger canting, which may further suggest the reduced periodicity, as is already discussed using neutron study [37] and is true for other rare-earth-based systems [60]. Needless to say, given the similarity in the crystal structure to MnSi, a positive Curie-Weiss temperature ($\theta_W \sim 9$ K) and a fluctuation-induced FO nature of the transition should not be overlooked and must be studied carefully using the magnetic sensitive techniques such as detailed ac susceptibility, magnetization, neutron diffraction, and scattering measurements, which may shed more light on the ground state. The other interesting observation in the *H-T* phase diagram is the presence of a tricritical point at around $H_{TCP} \sim 2.75$ T and $T_{TCP} \sim 3.2$ K. The deviation in the data points from the master curve in Fig. 9 is observed only for fields less than $H < 3$T and $\theta < -1$, which belongs to the temperature region below $T < 4$ K (marked as a dashed-dotted line in Fig. 12). This further suggests the field required to induce a SO PM-FP state lies between 2.75 and 3 T. Moreover, this puts an upper and lower limit on the tricritical temperature to be around $\sim 3.2$ and 2 K, respectively. However, considering the deviation in universal scaling above 2.75 T, the corresponding temperature obtained is 3.2 K, hence providing the tricritical point to be around $H_{TCP} \sim 2.75$ T and $T_{TCP} \sim 3.2$ K. The data points above $H > 4$ T in the phase diagram, marking the boundary of the SO phase transition between PM-FP, were taken from $\Delta\rho/\Delta\rho_{min}$ [Fig. 8(b)] and are extrapolated below $H < 4$ T to the tricritical point. Although EuPtSi and MnSi show many similarities in their properties, they still may belong to two different universality classes.

### IV. CONCLUSIONS

Summarizing the present study, a detailed and systematic study on EuPtSi is presented, giving special emphasis to the *H-T* phase diagram. The $A$ phase is established

using precise electrical resistivity and heat capacity measurements as a function magnetic field, which demonstrates the thermodynamic stability of the phase. The unique observation in the present study points towards the HM ground state below $T_N$ as well as the presence of a conclusive tricritical point in the $H$-$T$ phase diagram. The PM-HM transition below $T_N$, similar to MnSi, is argued based on a clear signature of the phase observed below $H_{C1}$ in $C(H)$ and $\rho(H)$ measurements. The universal MCE scaling evidences a first order to a field-induced second-order transition and a corresponding tricritical point at $H_{TCP} \sim 2.75\,T - T_{TCP} \sim 3.2\,K$. Moreover, the critical exponents obtained in the high-field region above $H > 4$ T suggest the EuPtSi belongs to a mean-field universality class different from MnSi, which belongs to the tricritical mean-field universality class.

[1] S. Mühlbauer, B. Binz, F. Jonietz, C. Pfleiderer, A. Rosch, A. Neubauer, R. Georgii, and P. Böni, Science **323**, 915 (2009).

[2] M. Uchida, N. Nagaosa, J. P. He, Y. Kaneko, S. Iguchi, Y. Matsui, and Y. Tokura, Phys. Rev. B **77**, 184402 (2008).

[3] W. Münzer, A. Neubauer, T. Adams, S. Mühlbauer, C. Franz, F. Jonietz, R. Georgii, P. Böni, B. Pedersen, M. Schmidt, A. Rosch, and C. Pfleiderer, Phys. Rev. B **81**, 041203(R) (2010).

[4] X. Z. Yu, Y. Onose, N. Kanazawa, J. H. Park, J. H. Han, Y. Matsui, N. Nagaosa, and Y. Tokura, Nature (London) **465**, 901 (2010).

[5] S. Seki, X. Z. Yu, S. Ishiwata, and Y. Tokura, Science **336**, 198 (2012).

[6] T. Adams, A. Chacon, M. Wagner, A. Bauer, G. Brandl, B. Pedersen, H. Berger, P. Lemmens, and C. Pfleiderer, Phys. Rev. Lett. **108**, 237204 (2012).

[7] Y. Tokunaga, X. Z. Yu, J. S. White, H. M. Rønnow, D. Morikawa, Y. Taguchi, and Y. Tokura, Nat. Commun. **6**, 7638 (2015).

[8] X. Z. Yu, N. Kanazawa, Y. Onose, K. Kimoto, W. Z. Zhang, S. Ishiwata, Y. Matsui, and Y. Tokura, Nat. Mater. **10**, 106 (2011).

[9] Y. Li, N. Kanazawa, X. Z. Yu, A. Tsukazaki, M. Kawasaki, M. Ichikawa, X. F. Jin, F. Kagawa, and Y. Tokura, Phys. Rev. Lett. **110**, 117202 (2013).

[10] Y. Ishikawa, K. Tajima, D. Bloch, and M. Roth, Solid State Commun. **19**, 525 (1976).

[11] A. Neubauer, C. Pfleiderer, B. Binz, A. Rosch, R. Ritz, P. G. Niklowitz, and P. Böni, Phys. Rev. Lett. **102**, 186602 (2009).

[12] A. Bauer and C. Pfleiderer, Phys. Rev. B **85**, 214418 (2012).

[13] S. S. Samatham and V. Ganesan, Phys. Status Solidi RRL **7**, 184 (2013).

[14] A. Bauer, M. Garst, and C. Pfleiderer, Phys. Rev. Lett. **110**, 177207 (2013).

[15] A. N. Bogdanov and D. A. Yablonskii, Zh. Eksp. Teor. Fiz. **95**, 178 (1989).

[16] A. N. Bogdanov and A. Hubert, J. Magn. Magn. Mater. **138**, 255 (1994).

[17] I. Kézsmárki, S. Bordács, P. Milde, E. Neuber, L. M. Eng, J. S. White, H. M. Rønnow, C. D. Dewhurst, M. Mochizuki, K. Yanai, H. Nakamura, D. Ehlers, V. Tsurkan, and A. Loidl, Nat. Mater. **14**, 1116 (2015).

[18] Y. Fujima, N. Abe, Y. Tokunaga, and T. Arima, Phys. Rev. B **95**, 180410(R) (2017).

[19] A. K. Nayak, V. Kumar, P. Werner, E. Pippel, R. Sahoo, F. Damay, U. K. Rößler, C. Felser, and S. S. P. Parkin, Nature (London) **548**, 561 (2017).

[20] C. Pfleiderer, G. J. MeMullan, and G. G. Lonzarich, Phys. B: Condens. Matter **199**, 634 (1994).

[21] A. Bauer, A. Neubauer, C. Franz, W. Münzer, M. Garst, and C. Pfleiderer, Phys. Rev. B **82**, 064404 (2010).

[22] C. Pfleiderer, G. J. McMullan, S. R. Julian, and G. G. Lonzarich, Phys. Rev. B **55**, 8330 (1997).

[23] L. D. Landau, Sov. Phys. JETP **35**, 70 (1959).

[24] S. S. Samatham, S. Yadam, D. Singh, and V. Ganesan, J. Magn. Magn. Mater. **418**, 289 (2016).

[25] A. K. Mishra, M. Krishnan, D. Singh, S. S. Samatham, M. Gangrade, R. Venkatesh, and V. Ganesan, J. Magn. Magn. Mater. **448**, 130 (2018).

[26] S. S. Samatham and V. Ganesan, Phys. Rev. B **95**, 115118 (2017).

[27] V. Franco, J. S. Blázquez, and A. Conde, Appl. Phys. Lett. **89**, 222512 (2006).

[28] V. Franco, A. Conde, J. M. Romero-Enrique, and J. S. Blázquez, J. Phys.: Condens. Matter **20**, 285207 (2008).

[29] C. M. Bonilla, J. Herrero-Albillos, F. Bartolomé, L. M. García, M. P. Borderías, and V. Franco, Phys. Rev. B **81**, 224424 (2010).

[30] Y. Su, Y. Sui, J.-G. Cheng, J.-S. Zhou, X. Wang, Y. Wang, and J. B. Goodenough, Phys. Rev. B **87**, 195102 (2013).

[31] V. K. Pecharsky and K. A. Gschneidner, Jr., Phys. Rev. Lett. **78**, 4494 (1997).

[32] A. Fert, V. Cros, and J. Sampaio, Nat. Nanotechnol. **8**, 152 (2013).

[33] X. Z. Yu, N. Kanazawa, W. Z. Zhang, T. Nagai, T. Hara, K. Kimoto, Y. Matsui, Y. Onose, and Y. Tokura, Nat. Commun. **3**, 988 (2012).

[34] M. Kakihana, D. Aoki, A. Nakamura, F. Honda, M. Nakashima, Y. Amako, S. Nakamura, T. Sakakibara, M. Hedo, T. Nakama, and Y. Ōnuki, J. Phys. Soc. Jpn. **87**, 023701 (2018).

[35] D. Adroja, B. Padalia, S. Malik, R. Nagarajan, and R. Vijayaraghavan, J. Magn. Magn. Mater. **89**, 375 (1990).

[36] D. G. Franco, Y. Prots, C. Geibel, and S. Seiro, Phys. Rev. B **96**, 014401 (2017).

[37] K. Kaneko, M. D. Frontzek, M. Matsuda, A. Nakao, K. Munakata, T. Ohhara, M. Kakihana, Y. Haga, M. Hedo, T. Nakama, and Y. Ōnuki, J. Phys. Soc. Jpn. **88**, 013702 (2019).

[38] J. M. Hopkinson and H.-Y. Kee, Phys. Rev. B **74**, 224441 (2006).

[39] S. V. Isakov, J. M. Hopkinson, and H.-Y. Kee, Phys. Rev. B **78**, 014404 (2008).

[40] T. E. Redpath and J. M. Hopkinson, Phys. Rev. B **82**, 014410 (2010).

[41] M. Kakihana, K. Nishimura, Y. Ashitomi, T. Yara, D. Aoki, A. Nakamura, F. Honda, M. Nakashima, Y. Amako, Y. Uwatoko, T. Sakakibara, S. Nakamura, T. Takeuchi, Y. Haga, E. Yamamoto, H. Harima, M. Hedo, T. Nakama, and Y. Ōnuki, J. Electron. Mater. **46**, 3572 (2017).

[42] I. I. Lobanova, V. V. Glushkov, N. E. Sluchanko, and S. V. Demishev, Sci. Rep. **6**, 22101 (2016).

[43] S. X. Huang, F. Chen, J. Kang, J. Zang, G. J. Shu, F. C. Chou, and C. L. Chien, New J. Phys. **18**, 065010 (2016).

[44] E. S. R. Gopal, *Specific Heats at Low Temperatures* (Springer, New York, 1966).

[45] P. Gegenwart, J. Custers, C. Geibel, K. Neumaier, T. Tayama, K. Tenya, O. Trovarelli, and F. Steglich, Phys. Rev. Lett. **89**, 056402 (2002).

[46] K. Heuser, E.-W. Scheidt, T. Schreiner, and G. R. Stewart, Phys. Rev. B **57**, R4198(R) (1998).

[47] G. R. Stewart, Rev. Mod. Phys. **73**, 797 (2001).

[48] Z. Hossain, C. Geibel, N. Senthilkumaran, M. Deppe, M. Baenitz, F. Schiller, and S. L. Molodtsov, Phys. Rev. B **69**, 014422 (2004).

[49] S. Danzenbächer, D. V. Vyalikh, Yu. Kucherenko, A. Kade, C. Laubschat, N. Caroca-Canales, C. Krellner, C. Geibel, A. V. Fedorov, D. S. Dessau, R. Follath, W. Eberhardt, and S. L. Molodtsov, Phys. Rev. Lett. **102**, 026403 (2009).

[50] M. Ge, L. Zhang, D. Menzel, H. Han, C. Jin, C. Zhang, L. Pi, and Y. Zhang, J. Alloys Compd. **649**, 46 (2015).

[51] M. K. Chattopadhyay, P. Arora, and S. B. Roy, J. Phys.: Condens. Matter **21**, 296003 (2009).

[52] L. Zhang, D. Menzel, C. Jin, H. Du, M. Ge, C. Zhang, L. Pi, M. Tian, and Y. Zhang, Phys. Rev. B **91**, 024403 (2015).

[53] B. Widom, J. Chem. Phys. **43**, 3898 (1965).

[54] R. B. Griffiths, Phys. Rev. **158**, 176 (1967).

[55] S. N. Kaul, J. Magn. Magn. Mater. **53**, 5 (1985).

[56] D. Fuchs, M. Wissinger, J. Schmalian, C. L. Huang, R. Fromknecht, R. Schneider, and H. v. Lohneysen, Phys. Rev. B **89**, 174405 (2014).

[57] N. Khan, A. Midya, K. Mydeen, P. Mandal, A. Loid, and D. Prabhakaran, Phys. Rev. B **82**, 064422 (2010).

[58] I. Dzyaloshinsky, J. Phys. Chem. Solids **4**, 241 (1958).

[59] T. Moriya, Phys. Rev. **120**, 91 (1960).

[60] T. Matsumura, Y. Kita, K. Kubo, Y. Yoshikawa, S. Michimura, T. Inami, Y. Kousaka, K. Inoue, and S. Ohara, J. Phys. Soc. Jpn. **86**, 124702 (2017).